Phase Analysis of Lock-Exchange Gravity Currents

Helena I.S. Nogueira, Claudia Adduce, Elsa Alves and Mário J. Franca

Department of Civil Engineering & IMAR-CMA,
University of Coimbra, Portugal
hnogueira@dec.uc.pt

Department of Civil Engineering
University of Rome, "Roma Tre", Italy
adduce@uniroma3.it

Department of Hydraulics and Environment
National Laboratory of Civil Engineering, Lisbon, Portugal
ealves@lnec.pt

Department of Civil Engineering & IMAR-CMA
New University of Lisbon, Portugal
mfranca@fct.unl.pt

Abstract

An image analysis technique is used to evaluate time-space varying density distribution of unsteady density currents produced by full-depth lock-release of saline water. Density currents with four initial densities were generated in a 3.0 m long, 0.20 m wide and 0.30 m deep flume, with horizontal smooth bed, and recorded with a 25 Hz CCD video camera. Using dye concentration as a tracer, a calibration procedure was applied for each pixel in the image relating an amount of dye uniformly distributed in the channel and grey scale values in the corresponding images. Subsequently, the quantity of dye is converted into salt concentration allowing the estimation of the 2D instantaneous current density distribution. Temporal evolution of the current front position and front velocity are analysed and related to different phases of the current development. Different Froude numbers, accounting for the initial and local reduced gravity and established with different length scales, are the non-dimensional form of the front velocity and help defining the ruling quantities on each phase.

1. Introduction

Gravity or density currents are flows driven by density differences within a fluid which can be due to temperature differences, dissolved substances or particles in suspension. Thunderstorms outflows, sea-breeze fronts, avalanches of airborne snow and plumes of pyroclasts from volcanic eruptions are examples of density currents in the atmosphere. In the water, one may refer oceanic fronts, dense overflows and turbidity currents (Simpson 1997). The latter may occur as a result of human intervention (release of mineral waste, dredging operations or debris from manmade structures collapses) or spontaneously in nature (flood events, earthquakes) in natural and manmade lakes and in the deep ocean, with significant morphological impacts. Gravity currents have important applications in aircraft safety, atmospheric pollution and dense gas technology (Simpson 1982). Density currents fed by contaminant materials dissolved or in suspension may have negative effects in terms of water quality in reservoirs and lakes. The loss of storage in reservoirs, related to the deposition of fine sediments due to turbidity currents, is a subject of great concern to hydraulic engineers and still a topic of research nowadays (Fan and Morris 1992; Kantoush et al. 2010; Alves et al. 2008). In the last 30 years advances have been made on the analysis of the physics of

density currents, both by using experimental (Rottman and Simpson 1983; Altinakar 1993; Lowe et al. 2002; Hogg et al. 2005; Cenedese and Adduce 2008) and numerical modelling (Härtel et al. 2000; Ooi et al. 2007; Paik et al. 2009; Bombardelli et al. 2009). Gravity currents produced by instantaneous releases of a fixed quantity of fluid within a finite channel present two, or even three, distinct phases: slumping phase, self-similar phase and a viscous phase (Simpson 1997; Rottman and Simpson 1983). After the instantaneous release, simulated by means of a gate sudden removal, an initial adjustment phase is observed, during which the front position varies linearly with time, i.e., the front advances with approximately constant velocity (Rottman and Simpson 1983). This first phase merges into a second phase when a disturbance generated at the end wall overtakes the front. From this instant, the front speed decreases as $t^{-1/3}$. When viscous effects begin to dominate inertial effects, a third phase develops and the current front velocity decreases even more rapidly (as $t^{-4/5}$). Several studies have been developed through image analysis technique to investigate the dynamics of gravity currents (Marino et al. 2005; La Rocca et al. 2008; Adduce et al. 2009); the present research, based on experimental work, uses similar techniques (Nogueira 2011).
The present work aims at (i) identifying the phases of current development for four different initial densities in the lock, (ii) defining the length of the current head and, finally, (iii) analysing characteristic variables for each phase of the current, namely by comparing different kinematic scales, bulk and local (these latter characterizing the current head), for normalization of the front velocity (different Froude numbers analysis). The research is based on experimental work where lock-exchange density currents are reproduced under controlled conditions on an open-channel. The development of the current is captured by a 25 Hz CCD camera, using dye concentration as a tracer, allowing thus the reconstruction of time space (2D) evolution of the density fields.
After this introduction, experimental details are given in section 2, main results concerning front velocity and position, current dimensions and Froude numbers are presented and discussed in section 3 and section 4 is devoted to the main conclusions.

2. Experimental details

The lock-release experiments were performed in a 3.0 m long transparent Perspex channel with a 0.2 m wide and 0.3 m deep rectangular cross-section (Fig. 1) at the Hydraulics Laboratory of University of Rome, “Roma Tre”.

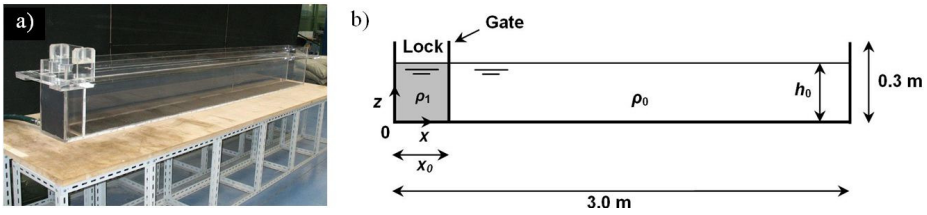

Figure 1: Perspex channel: a) perspective photo and b) longitudinal view.

A vertical sliding gate is placed in the channel at a distance x_0 = 0.15 m from the left wall to form a lock. The right side of the channel is filled with fresh water with density ρ_0, whereas the lock is filled with saline water with density ρ_1; both sides filled up at same depth, h_0 = 0.20 m. The channel bed is smooth (Perspex roughness $\varepsilon \approx 0$ mm) and horizontal. The density of the saline water is controlled by a pycnometer being the error of the weighing apparatus 0.05%. A controlled quantity of white colorant is added to the mixture in the lock to provide flow visualization. We assume that the colorant does not influence the density of the saline mixture. The outside back wall of the channel is lined with black paperboard to produce a dark, uniform background to contrast with the white dyed developing gravity current. At the

beginning of each experiment the gate is suddenly removed, leaving the dense fluid to flow under the fresh water.
The evolution of the gravity current is recorded by a CCD video camera SONY XC-77CE with 768 x 576 pixels of resolution and frequency of 25 Hz. The camera is kept at a fixed perpendicular position 5.8 m from the channel and aligned with its centre to capture the whole channel length. A metric scale is positioned in both horizontal and vertical directions of the channel and used for geometric calibration. The illumination is made by means of artificial light. During the experiments, the upper part of the channel is covered with a thin black painted wooden board to avoid reflection of light from the water surface. The video frames were subsequently converted into gray scale matrices in the region of the channel with fluid (702 x 43 pixels) and then converted into instantaneous density fields of the current through a calibration procedure. Results are shown for a selected window (dashed rectangle in Fig. 2) of the field of view, avoiding the influence of the disturbed flow near the gate.

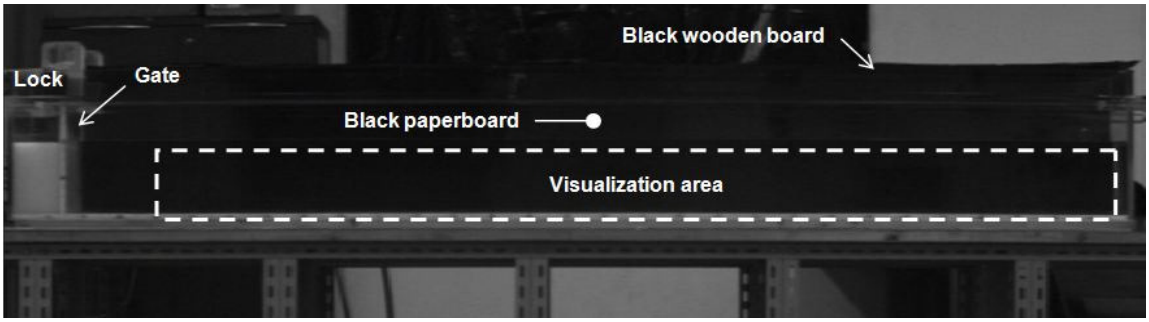

Figure 2: Lateral view of the channel and region analysed further in the text.

The evaluation of the current density distribution was based on Hacker et al. (1996) technique, which relates light intensity through the current with the concentration of dye present in the flow; this latter is considered linearly correlated with salt concentration within the current body. A calibration procedure was carried out for each single pixel in the region defined earlier (702 x 43 pixels), to establish the relation between the amount of dye in the water and the values of gray scale in the frames representing light intensities. We assume that salt dissolved in water does not change significantly the light absorption, thus is sufficient to look at dye concentration for calibration purposes. Eight known dye quantities, increasingly from zero to a maximum value corresponding to ρ_1, were uniformly distributed through the channel being the corresponding images captured for calibration for the very same light conditions and distance between camera and channel as during the experiments. Gray scale values increase nonlinearly with the amount of dye in the flow. Assuming a direct relation between the amount of dye and the density of the current, it is thus possible to infer density values at any given pixel and at any given instant from its instantaneous gray scale value. This procedure is then verified through total salt mass conservation principle applied to the entire experimental channel, accounting thus with the current mass and the mass of ambient fluid.
Fig. 3 shows a photo of the current acquired at t = 27 s ($tu_b/x_0 = 31$, u_b is the buoyancy velocity defined latter in the text) after the gate removal in run 1 (experimental runs defined in Table 1) and the correspondent plot of iso-density contours plotted for $\rho^* = 0.015$, 0.10, 0.25 and 0.40, being ρ^* the instantaneous 2D local non-dimensional density defined as

$$\rho^* = \frac{\rho(x,z,t) - \rho_0}{\rho_1 - \rho_0} \tag{1}$$

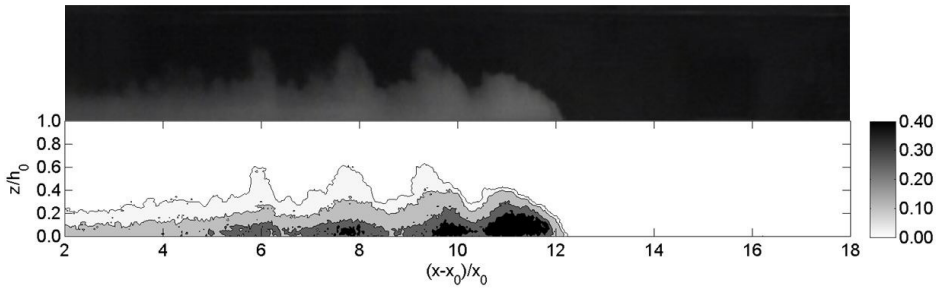

Figure 3: (top) Photo of the current acquired at t = 27 s (tu_b/x_0 = 31) after the gate removal in run 1; (bottom) iso-density contours plotted at ρ^* = 0.015, 0.10, 0.25 and 0.40.

Each test was performed for an initial reduced gravity of the mixture in the lock, defined as

$$g' = g\,\frac{(\rho_1 - \rho_0)}{\rho_0} \tag{2}$$

being ρ_1 the initial density of the saline water and ρ_0 the density of the ambient fluid. Main parameters are presented in the non-dimensional form by adopting the following dimensionally independent scales, in accordance with previous studies (Hacker et al. 1996, Marino et al. 2005): lock length x_0 as length scale, buoyancy velocity defined as

$$u_b = \sqrt{g'\,h_0} \tag{3}$$

as velocity scale, where h_0 is the initial water depth in the channel. Table 1 gives the main parameters of experiments showing as well symbols used subsequently to their representation.

Table 1: Main parameters of the experiments.

Run	ρ_1 (kgm^{-3})	g' (ms^{-2})	u_b (ms^{-1})	Symbols in figures
1	1015	0.147	0.172	○
2	1030	0.294	0.243	□
3	1045	0.441	0.297	▲
4	1060	0.589	0.343	*

Time-varying Froude number, based on the front velocity, defined as

$$Fr = \frac{u_f}{\sqrt{g'\,h}} \tag{4}$$

was computed using three different length scales, i.e. characteristic heights, h, of the current: h_0, maximum height of the head h_m and height at the rear of the head h_r. Froude numbers so obtained were compared with the local Froude number of the head region defined as

$$Fr_{head} = \frac{u_f}{\sqrt{g_{head}'\,h}} \tag{5}$$

where g'_{head} is the local reduced gravity computed by using the head-averaged density of the current at each instant. Similarly, the very same three different depths h were used as characteristic heights: h_0, h_m and h_r. The boundary between the current and the ambient fluid was defined by adopting a non-dimensional density threshold of ρ^* = 0.01.

3. Results

3.1 Front position and velocity

The instantaneous front position $x_f(t)$ was estimated through the instantaneous density maps

by taking the x-position of the foremost point of the current. Fig. 4a shows the variation with time of non-dimensional front position and Fig. 4b the corresponding log-log plot for all runs.

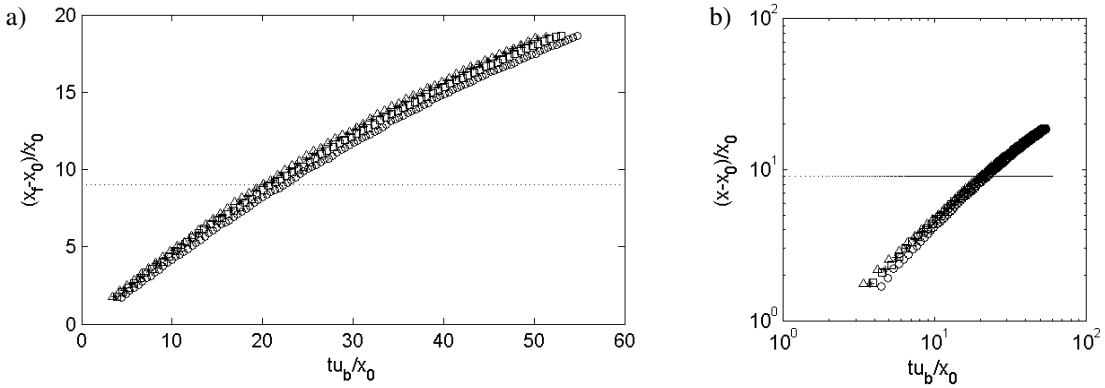

Figure 4: Temporal evolution of the non-dimensional current front position for each run (symbols explained in Table 1).

Fig. 4 shows data collapsing in one cloud when normalized by kinematic parameters earlier introduced. Two distinct phases are observed for the development of the gravity current in all runs. The first phase, characterized by a linear relation between front position and time after the gate removal, is observed till roughly $(x_f-x_0)/x_0 \approx 8.2$, a value slightly lower than the described in literature (Rottman and Simpson 1983). Transition points between first and second phases were estimated by applying a linear regression to $x_f(t)$ data by a least-squares approach. Second phase $x_f(t)$ data was adjusted by a power law of type $x_f=at^b$. Coefficients a and b were obtained through a least-squares regression applied after data linearization. Table 2 summarizes main characteristics of each phase for all runs. Values of front velocity herein shown were obtained by derivation of the regression function adjusted to the first phase.

Table 2: Main characteristics of different phases of development for lock-exchange gravity currents (t_{f1} and x_{f1} are the time and space coordinate corresponding to the transition between first and second phase and u_{f1} the velocity during the first phase).

Run	first phase				second phase	
	$t_{f1}u_b/x_0$	$(x_{f1}-x_0)/x_0$	u_{f1} (ms^{-1})	u_{f1}/u_b	a	b
1	20.8	8.5	0.071	0.414	0.74	0.81
2	14.7	6.6	0.111	0.458	0.74	0.81
3	18.1	8.4	0.141	0.475	0.90	0.78
4	20.4	9.1	0.156	0.455	0.81	0.78

In the slumping (first) phase, velocity is roughly constant being the average non-dimensional value, normalized by the buoyancy velocity, around 0.45, corroborating previous results. In the so-called self-similar (second) phase, linearized front position data collapse well and consistently around a straight line with slope around 0.80 (Table 2), which is slightly higher than the value of 2/3 predicted in the literature. The channel where the experiments were performed is 3.0 m long, thus no viscous phase was observed in accordance with previous results patent in the literature (Rottman & Simpson 1983).

3.2 Definition of the current head

Since the head of the density current is the region where higher density is observed, the criteria used to characterize and isolate this region was based on a function given by the product between local values of depth-averaged density in each vertical and current height:

$$W(x,t) = \overline{\rho}_v(x,t)h(x,t) \tag{6}$$

which corresponds to local vertically-averaged mass of the current. The upstream limit of the head, and therefore the head length L_f, were defined taking the position of the first meaningful local minimum of function w (6) above defined, near the front. Figure 5 shows a scheme of the current with the characteristic variables of the head.

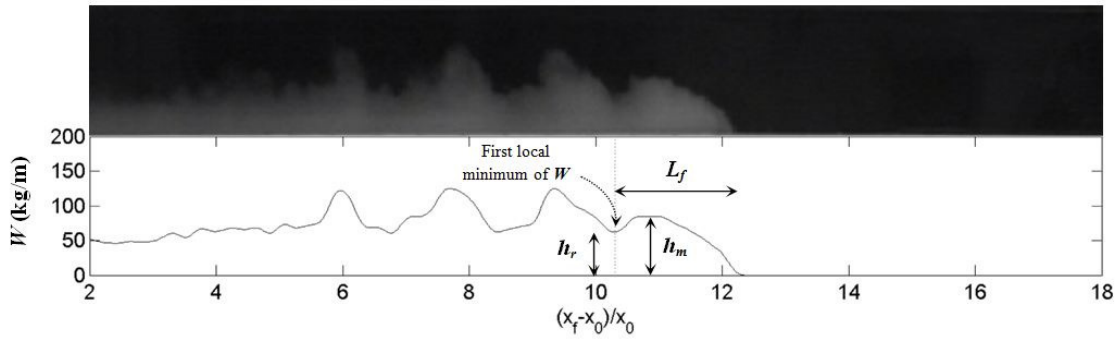

Figure 5: Definition of the head of the density current and its characteristic variables.

3.3 Similitude analysis

Fig. 6 shows different Froude numbers computed with bulk initial reduced gravity –equation (4) and local reduced gravity – equation (5) (left and right, respectively), and for the three different above mentioned depths used as length scale – h_0, h_m and h_r (a to c, respectively).
Velocities are taken from derivation of regression curves (Table 2) applied to $x_f(t)$ position data. As expected, results are sparser when using local normalizing variables. Data exhibit a better collapse when using reduced gravity (left side), thus initial reduced gravity of the mixture in the lock seems more appropriated to normalize front velocities. Also, using bulky h_0 instead of local length scales seems to produce better results in terms of data collapse (phenomenon similitude). Nevertheless, similar trends are observed when comparing left and right plots from Fig. 6. For Froude numbers estimated with h_0 (6a), a constant plateau around Fr_{h0}=0.45 is observed, in agreement with what is reported in literature (Marino et al 2005). When normalizing by local reduced gravity (right side), time and space varying head reduced gravity affects results and similitude in Fr_{h0} is hardly observed – these varies roughly between 0.6 and 0.9. An increasing trend is observed with the initial density in the lock, indicating and confirming velocity dependency on this parameter shown on the left side of Fig. 6a.
When using local length scale to calculated Froude numbers, Figs. 6b and c, data collapsing to a constant plateau seems more evident in the second phase, agreeing with previous observations. Both results, with h_r and h_m are similar, only slightly different in terms of amplitude due to the evident differences in these geometric values (cf. Fig. 5). Again, when normalizing with local reduced gravity, data similitude is poorer denoting again the influence of the initial density in the lock on the front propagation. This is corroborated as well by looking at the increase in Froude numbers results when initial density increases (Figs. 6b and c, right hand side). The sparse results when using local length scales, intrinsically related to the definition of the head dimensions (Fig. 5) maybe be due to the unstable character of the current head where a stretching-breaking cycle is observed (Nogueira et al. 2011).

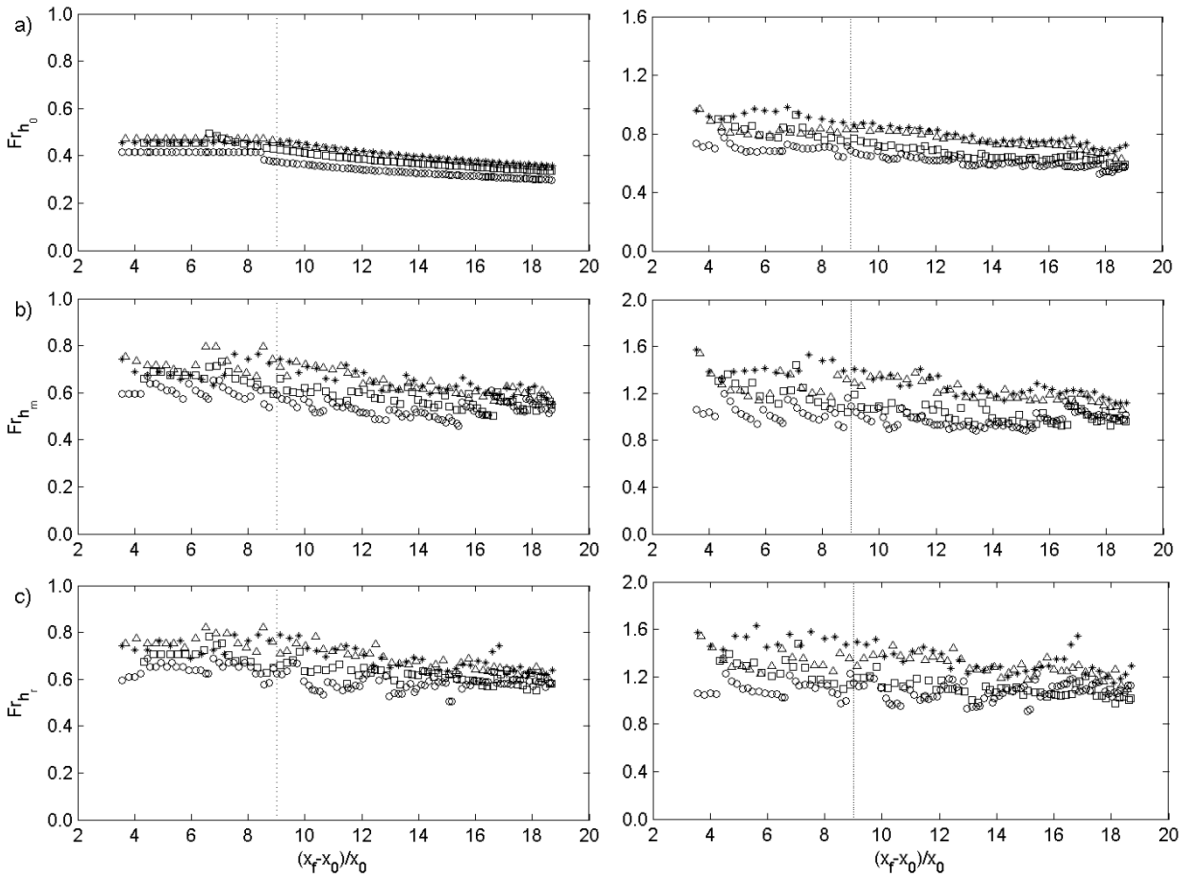

Figure 6: Evolution of Froude numbers considering (left) initial reduced gravity and (right) local reduced gravity, and using different characteristic heights defined as a) initial depth in the lock h_0, b) maximum height of the head h_m and c) height at the rear of the head h_r (symbols explained in Table 1).

4. Conclusions

Gravity currents produced by lock-release of saline water into a finite open-channel are presented and discussed in what concerns time evolution of the front and front velocity, and front propagation similitude (Froude numbers analysis). All tests show the development of the current in two distinct phases, is in agreement with the literature for lock-exchange flows with akin characteristics. Results confirm that in the first phase front velocities are nearly constant (linear evolution of front position). Transition points between first (slumping) and second (self-similar) phases were obtained in the range $(x_f-x_0)/x_0 \approx 6.6$ to 9.1, near of predictions in literature. In the self-similar phase, front position is a function of $t^{0.8}$, approximately; the exponent is higher than what is described in literature (2/3). When normalizing front velocity with bulk variables (initial reduced gravity of the mixture in the lock and initial water depth in the channel), similitude in the first phase is attained and comparable with previous results. When using current head reduced gravity, results are sparser and show an influence of the initial density in the lock, corroborating this as a ruling variable on these flows.

Acknowledgments

This research was supported by the Portuguese Science and Technology Foundation (FCT) through the research project PTDC/ECM/099752/2008 and the research grant SFRH/BD/48705/2008.

References

Adduce, C., Lombardi, V., Sciortino, G. and Morganti, M. (2009) Roughness effects on gravity currents dynamics. *33rd IAHR Congress*, Vancouver, August 9-14, 2009.

Altinakar, M.S. (1993) Weakly depositing turbidity currents on small slopes. *Dissertation, École Polytechnique Fédérale de Lausanne (EPFL)*, Lausanne, Switzerland.

Alves, E., González, J., Freire, P. and Cardoso, A.H. (2008) Experimental study of plunging turbidity currents in reservoirs. *River Flow 2008*, Cesme-Izmir, September, 2008.

Bombardelli, F.A., Cantero, M.I., García, M.H. and Buscaglia, G.C. (2009) Numerical aspects of the simulation of discontinuous saline underflows: the lock-exchange problem. *J Hydr Res*, 47(6):777-789.

Cenedese, C. and Adduce, C. (2008) Mixing in a density-driven current flowing down a slope in a rotating fluid. *J Fluid Mech*, 604:369-388.

Fan, J. and Morris, G.L. (1992a) Reservoir sedimentation I: Delta and density current deposits. *J Hydr Eng*, 118(3):354-369.

Fan, J. and Morris, G.L. (1992b) Reservoir sedimentation II: Reservoir desiltation and long-term storage capacity. *J Hydr Eng*, 118(3):370-384.

Hacker, J., Linden, P.F. and Dalziel, S.B. (1996) Mixing in lock-release gravity currents. *Dyn Atmos Oceans* 24:183-195.

Härtel, C., Meiburg, E. and Necker, F, (2000) Analysis and direct numerical simulation of the flow at a gravity-current head. Part 1. Flow topology and front speed for slip and no-slip boundaries. *J Fluid Mech*, 418:189-212.

Hogg, A.J., Hallworth, M.A. and Huppert, H.E. (2005) On gravity currents driven by constant fluxes of saline and particle-laden fluid in the presence of a uniform flow. *J Fluid Mech*, 539:349-385.

Kantoush, S.A., Sumi, T. and Murasaki, M. (2010) Evaluation of sediment bypass efficiency by flow field and sediment concentration monitoring techniques. *Annua J Hydr Eng*, 55.

La Rocca, M., Adduce, C., Sciortino, G. and Pinzon, A.B. (2008) Experimental and numerical simulation of three-dimensional gravity currents on smooth and rough bottom. *Physics of Fluids*, 20.

Lowe, R.J., Linden, P.F. and Rottman, J.W. (2002) A laboratory study of the velocity structure in an intrusive gravity current. *J. Fluid Mech.*, 456:33-48.

Marino, B.M., Thomas, L.P. and Linden, P.F. (2005) The front condition for gravity currents. *J. Fluid Mech*., (536):49-78.

Nogueira, H.I.S. (2011) Time and space analysis of entrainment on density currents. *34th IAHR Congress*, Brisbane, June-July, 2011.

Nogueira H.I.S., Adduce C., Alves E. and Franca M.J. (2011) Analysis of the entrainment on lock-exchange density currents. *EGU General Assembly 2011*.

Ooi, S.K., Constantinescu, G. and Weber, L.J. (2007) 2D Large-eddy simulation of lock-exchange gravity current flows at high Grashof numbers. *J. Hydr Eng*, 133(9):1037-1047.

Paik, J., Eghbalzadeh, A. and Sotiropoulos, F. (2009) Tree-dimensional unsteady RANS modelling of discontinuous gravity currents in rectangular domains. *J. Hydr Eng*, 135(6):505:521.

Rottman, J.W. and Simpson, J.E. (1983) Gravity currents produced by instantaneous releases of a heavy fluid in a rectangular channel. *J. Fluid Mech.*, 135:95-110.

Simpson, J.E. (1982) Gravity currents in the laboratory, atmosphere, and ocean. *Annual Rev. Fluid Mech.*, 14:213-234.

Simpson, J.E. (1997) Gravity currents: in the environment and the laboratory. 2nd edn., *Cambridge University Press*, New York, pp 1-2.